Dalton Transactions

PAPER

View Article Online
View Journal | View Issue

Cite this: *Dalton Trans.*, 2015, **44**, 5331

A new photoactive Ru(II)tris(2,2′-bipyridine) templated Zn(II) benzene-1,4-dicarboxylate metal organic framework: structure and photophysical properties†

Christi L. Whittington, Lukasz Wojtas, Wen-Yang Gao, Shengqian Ma and Randy W. Larsen*

Received 26th August 2014,
Accepted 19th January 2015

DOI: 10.1039/c4dt02594f

www.rsc.org/dalton

It has now been demonstrated that Ru(II)tris(2,2′-bipyridine) (RuBpy) can be utilized to template the formation of new metal organic framework (MOF) materials containing crystallographically resolved RuBpy clusters with unique photophysical properties. Two such materials, RWLC-1 and RWLC-2, have now been reported from our laboratory and are composed of RuBpy encapsulated in MOFs composed of Zn(II) ions and 1,3,5-tris(4-carboxyphenyl)benzene ligands (C. L. Whittington, L. Wojtas and R. W. Larsen, *Inorg. Chem.*, 2014, **53**, 160–166). Here, a third RuBpy templated photoactive MOF is described (RWLC-3) that is derived from the reaction between Zn(II) ions and 1,4-dicarboxybenzene in the presence of RuBpy. Single Crystal X-ray diffraction studies determined the position of RuBpy cations within the crystal lattice. The RWLC-3 structure is described as a 2-fold interpenetrated pillared honeycomb network (**bnb**) containing crystallographically resolved RuBpy clusters. The two **bnb** networks are weakly interconnected. The encapsulated RuBpy exhibits two emission decay lifetimes (τ-fast = 120 ns, τ-slow = 453 ns) and a bathochromic shift in the steady state emission spectrum relative to RuBpy in ethanol.

Introduction

Metal organic frameworks (MOFs) are a class of materials that possess a number of important features critical to the design and development of new technologies for a wide range of applications, including gas storage and separation, heterogeneous catalysts and drug delivery.[1] The versatility of MOFs is due to the fact that these materials contain coordinate bonds between diverse metals or metal clusters (commonly referred to as molecular building blocks, MBBs) and multidentate organic ligands.[1]

Porous MOFs also offer enormous potential for the development of photoactive materials with applications in solar energy and/or solar photochemistry due to the fact that a wide variety of photoactive guest molecules can be accommodated within the vacant pores of the MOF and the framework itself can be constructed with photocatalytic elements.[2] In fact, photocatalytic MOFs have now been developed in which free base and metalloporphyrins as well as Ru(II)tris(2,2′-bipyridine) (RuBpy) have been encapsulated within a variety of MOFs.[3–6] In addition, numerous MOFs have also been developed in which the frameworks themselves contain photoactive building units or bridging ligands.[7]

The RuBpy-type complexes are of specific interest as guests in the development of photocatalytic MOFs due to the fact that the excited states of RuBpy exhibit favourable reduction/oxidation potentials, relatively long lifetimes (allowing for greater excited state reactivity) and excellent photostability.[8] In addition, a wide array of functionalized bipyridine ligands are available which can be utilized to further tune the excited state properties of the Ru(II)$(L)_3$-type complexes.[8] Encapsulation of RuBpy into zeolites or MOF materials also has a significant impact on the photophysical properties of the complex. For example, encapsulation of RuBpy into the polyhedral Zn(II) MOF USF2 resulted in a material in which the triplet metal-to-ligand charge transfer (^{3}MLCT) lifetime was significantly extended relative to the complex in solution ($\tau_{Ethanol}$ = 614 ns and τ_{USF2} = 1.2 μs at 25 °C).[4] The extended lifetime was attributed to a deactivation of a non-radiative triplet ligand field (^{3}LF) state that is anti-bonding with respect to the RuBpy due to a confined molecular environment.

Recently, we reported two new RuBpy-based photoactive materials derived from reactions between Zn(II) ions and 1,3,5,-tris(4-carboxyphenyl)benzene and templated by the

Department of Chemistry, University of South Florida, Tampa, Florida, USA.
E-mail: rwlarsen@usf.edu

† Electronic supplementary information (ESI) available. CCDC 1025134. For ESI and crystallographic data in CIF or other electronic format see DOI: 10.1039/c4dt02594f

presence of RuBpy (RWLC-1 and RWLC-2).[5] The RuBpy cations have been crystallographically resolved within the cavities (RWLC-1) and channels (RWLC-2) of the new negatively charged frameworks and display unique photophysical properties. RuBpy encapsulated in each of the two new MOFs exhibit two ^{3}MLCT emission decay lifetimes ($\tau_{RWLC\text{-}1\text{-}fast}$ = 237 ns, $\tau_{RWLC\text{-}1\text{-}slow}$ = 1.60 μs, $\tau_{RWLC\text{-}2\text{-}fast}$ = 171 ns and $\tau_{RWLC\text{-}2\text{-}slow}$ = 797 ns at 25 °C). The emission data are consistent with two populations of RuBpy complexes, one being encapsulated in highly space-restricted cavities and a second indicative of encapsulation within larger non-periodic pores or defect regions. The space restricted population displays long emission lifetimes as well as a possible ^{1}MLCT above the ^{3}MLCT manifold while the non-specifically bound population exhibits a short lifetime due to co-encapsulation of quencher molecules.

In order to explore the possibility of RuBpy entrapment within mesoporous/defect regions in MOF crystals we have attempted to adsorb/entrap RuBpy clusters within the prototypical MOF, MOF-5 which is known to contain such features.[9,10] The MOF-5 material is composed of a ZnO_4-type clusters linked by benzene-1,4-dicarboxylate ligands giving rise to an extended 3D cubic framework of 12 Å cavities interconnected through 8 Å diameter pores. The small pore size precludes encapsulation of the RuBpy complex which has a diameter of roughly ~12 Å due to van der Waals volume restrictions. However, in the presence of RuBpy the MOF-5 synthesis produced a new MOF, hereafter RWLC-3, containing crystallographically resolved RuBpy clusters also displaying unique photophysical properties.

Experimental

Synthesis of RWLC-3

The RWLC-3 material was prepared by the addition of benzene-1,4-dicarboxylic acid (BDC) (20 mg, 0.12 mmol) in 3 mL of a 1 : 1 (v/v) ethanol–dimethyformamide (EtOH–DMF) solution to $Zn(NO_3)_2{\cdot}6H_2O$ (35 mg, 0.12 mmol) in 0.5 mL H_2O. To this mixture was added 20 mg of RuBpy (chloride salt) followed by heating in a scintillation vial at 105 °C for 18 hours in an oil bath. Crystals (Fig. 1) were repeatedly washed with EtOH. Approximately 25 to 50 mg of crystals were recovered from the solution.

Steady state and time resolved emission

Crystals of the RWLC-3 material were immobilized on a glass slide with a thin layer of vacuum grease and placed into a cuvette containing a small amount of ethanol to prevent the crystals from drying. The cuvette was then deaerated with Ar gas. Steady state emission and polarization measurements were performed using an ISS PC1 single-photon counting spectrofluorimeter. Emission was measured 45° relative to the 450 nm excitation beam. Polarization values were an average of 30 individual measurements. Lifetime measurements were performed on the same cuvette in a variable temperature sample holder by excitation with a 7 ns laser pulse (FWHM) from a frequency doubled Continuum MiniLite II frequency doubled Nd:YAG laser (~1 mJ per pulse). Sample emission was collected 45° relative to the excitation beam with a focusing optic into an amplified Si-photo-diode (EOT, ~200 ps rise time) and digitized using a 4 GHz transient digitizer (Tektronix 7404). Collected data was analyzed with OriginPro8™.

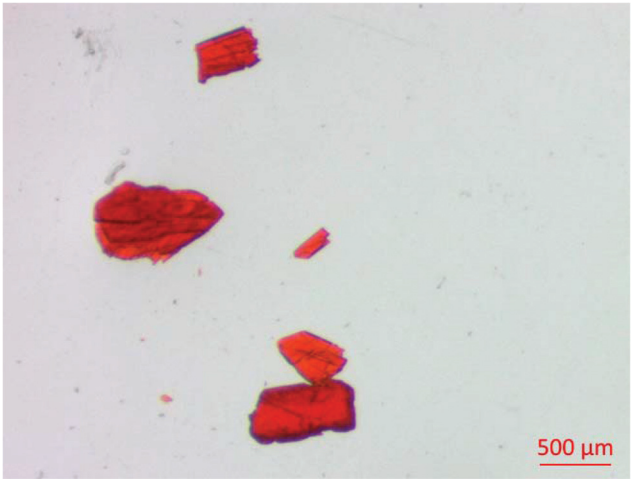

Fig. 1 Microscope images of RWLC-3 crystals. Images were obtained from a Zeiss SteREO Discovery V8 Microscope with an Achromat S 1.0× FWD 63 mm objective and 2× or 1.25× zoom. The microscope is equipped with a Digital Microscopy CMOS Camera AxioCam ERc 5s, 1×.

X-ray crystallography

The X-ray diffraction data for RWLC-3 were collected using Bruker D8 Venture PHOTON 100 CMOS diffractometer system equipped with a Cu Kα INCOATEC ImuS micro-focus source (λ = 1.54178 Å). Data have been processed using APEX2 software.[11] Structures have been solved using SHELXS-97 (direct methods) and refined using SHELXL-97 within the OLEX2 interface.[12] All non-H atoms have been found from difference Fourier map. The RuBpy is disordered over two positions around the inversion centre (1 : 1 ratio). One of the terephthalate ligands is disordered over two positions with 0.91 : 0.09 occupancy ratio. Solvent DMF or diethylamine (DEA, thermal breakdown product of DMF) molecules are disordered over at least five positions with one major position with 40% occupancy. More detailed description of the structure can be found in Result and discussion and ESI† of the manuscript.

Results and discussion

MOF structure

The structure of RWLC-3 contains RuBpy encapsulated within a framework described as 2-fold interpenetrated pillared honeycomb network (RCSR: **bbn**) (Fig. 2 and 3). The two **bbn** networks are interconnected through weak Zn···O coordination bonds between adjacent Zn clusters (Zn1···O distances: 2.43(8) Å for major part of the disorder, 91% and 2.36(8) Å for minor

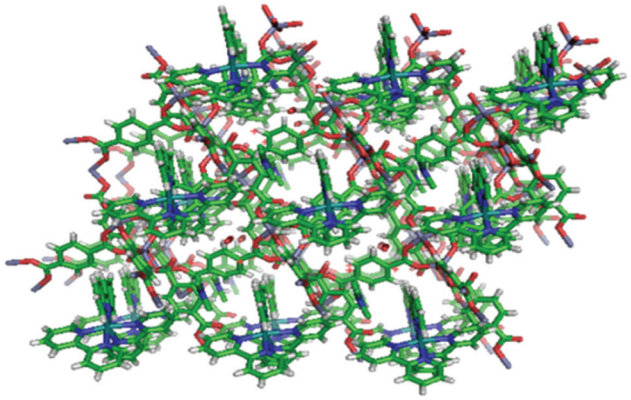

Fig. 2 Crystal structure of RWLC-3.

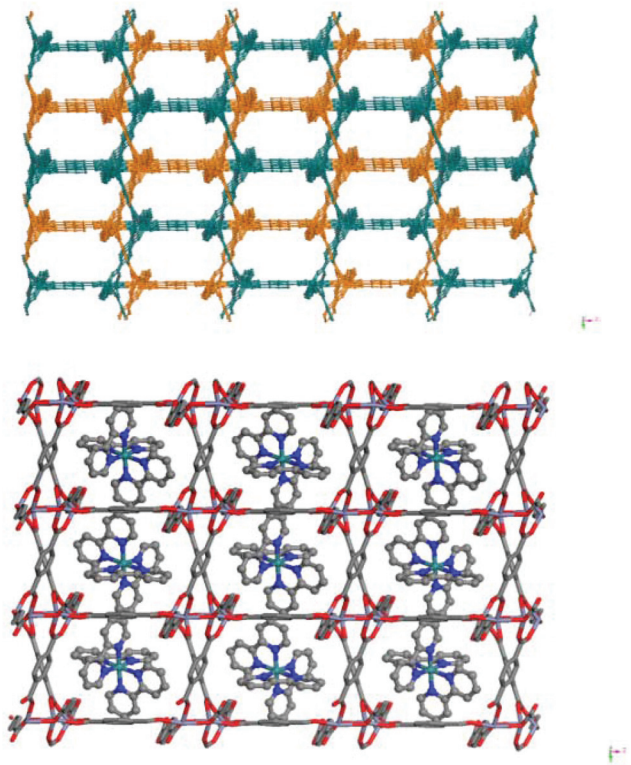

Fig. 3 Top panel: diagram showing the interpenetration of the bnb network of RWLC-3. Bottom panel: crystal structure illustrating the orientation of the RuBpy clusters.

part of the disorder, 9%). The single **bbn** network consists of trigonal Zn paddle wheel clusters at the honeycomb network vertices, which are connected through benzene-1,4-dicarboxylate anions. The honeycomb layers are axially connected at the vertices by terephthalate ligands to form a 3-D **bbn** network. The negatively charged framework is neutralized by RuBpy cations located within the channels. The RuBpy cation is disordered over two, well-resolved, positions around the inversion centre. The remaining free space is occupied by DMF/DEA molecules.

Steady state emission

The steady state emission spectrum of RWLC-3, displayed in Fig. 4, is bathochromically shifted by 6 nm relative to RuBpy in solution (612 nm *versus* 606 nm for RuBpy in ethanol) (Table 1 containes the emission maxima and polarization values for RWLC-1, RWLC-2 and RWLC-3 together with RuBpy in solution). The spectra of RWLC-3 and RuBpy in ethanol were fit to eqn (1):

$$I(E) = \sum_{n=0}^{N}\sum_{m=0}^{M}[(E_{00} - nh\omega_M - mh\omega_L)/E_{00}]^4(e^{-S_M}/n!)(e^{-S_L}/m!)\exp[-4\mathrm{Ln}2(E - E_{00} + nh\omega_h + mh\omega_l/\Delta\nu_{1/2})^2] \quad (1)$$

where $I(E)$ is the intensity at energy E, E_{00} is the emission energy, $\Delta\nu_{1/2}$ is the full width at half maximum of the E_{00} and other vibrational modes, n and m are the vibrational quantum numbers for medium and low frequency acceptor vibrational modes, S_M and S_L are the corresponding vibronic coupling factors, and $h\omega_M$ and $h\omega_L$ are the vibrational frequencies of the acceptor modes.[13] The results of the fits are summarized in Table 2. From fitting the experimental data the E_{00} value

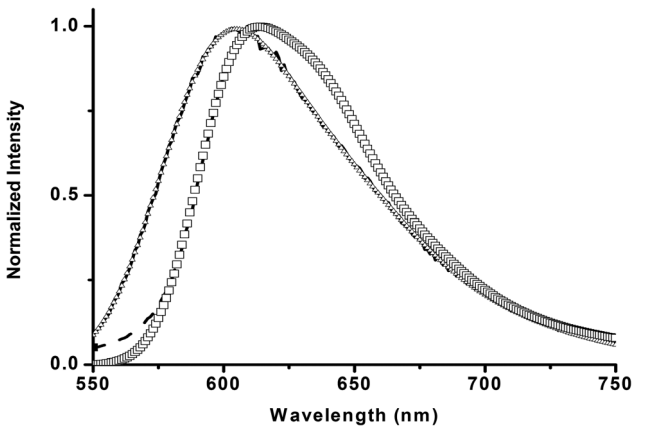

Fig. 4 Normalized steady state emission spectra of RuBpy in solution (squares) and RWLC-3 (triangles). Excitation wavelength was 450 nm. The solid lines are fit to eqn (1).

Table 1 Steady state emission maxima and polarization values at 25 °C

Compound	λ_{max} (nm)	Polarization
RuBpy in EtOH	606	0.005 ± 0.002
RWLC-3	612	0.13 ± 0.02
RWLC-1	583	0.26 ± 0.03
RWLC-2	626	0.49 ± 0.04

Table 2 Parameters obtained from fitting steady state emission data to eqn (1). E_{00}, $h\omega_M$, $h\omega_L$, and $\Delta\nu_{1/2}$ are in cm^{-1}

Sample	E_{00}	$h\omega_M$	$h\omega_L$	S_M	S_L	$\Delta\nu_{1/2}$	χ^2
RuBpy in EtOH	16 910	1278	294	0.61	0.93	1552	0.004
RWLC-3	16 524	2471	846	0.14	0.19	1076	0.012

associated with the closely spaced ^{3}MLCT manifold was found to be 16 910 cm^{-1} for RWLC-3 relative to 16 524 cm^{-1} for RuBpy in ethanol. The reduction of the ^{3}MLCT manifold zero point energy may arise from several factors. First, formation of the ^{3}MLCT manifold gives rise to a large change in dipole moment resulting in significant solvent reorganization in solution.[8] Changes in local solvation may provide additional stabilization of the charge transfer complex thus lowering the E_{00}. In addition, the framework metal clusters can modulate the magnitude of the RuBpy dipole moment also affecting the magnitude of E_{00}. Computational studies are currently underway to determine specific structural features affecting the ^{3}MLCT manifold E_{00} values. The fitting also revelaes significant differences in high and low frequency acceptor modes and vibronic coupling factors that are likely do to framework contacts with the RuBpy clusters.

The emission polarization is described by:

$$(1/P - 1/3) = (1/P_0 - 1/3)(1 + \tau/\phi) \quad (2)$$

where P is the measured polarization, P_0 is the limiting polarization, τ is the natural lifetime and ϕ is the rotational correlation time. Since ϕ = 1/6D (where D is the lateral diffusion time) the value of $(\tau/\phi) \rightarrow 0$ for large D systems such as the RWLC-1, -2 and -3 structures and $P = P_0$.[14] The P_0 term is related to the angle, θ, between the absorption and emission dipole moments by:

$$P_0 = [3 <\cos^2 \theta> -1]/[<\cos^2 \theta> + 3]. \quad (3)$$

In the case of the RuBpy complex isolated in solid matrices, the polarization value varies with excitation wavelength across the ^{3}MLCT absorption band.[15,16] The highest value is ~0.20 with an excitation wavelength of 470 nm while excitation over a range from 455 nm to 435 nm gives a polarization of ~0.14. This polarization value has been suggested to arise from a weak linearly polarized $^1A_1 \rightarrow {}^1A_2$ excitation together with a plane polarized $^1A_1 \rightarrow {}^1E$ excitation followed by a plane polarized $^3E \rightarrow {}^1A_1$ emission (under D_3 symmetry).[15–17] The similarity in the polarization values between RuBpy in solid ZnBpy matrices and RWLC-3 suggest a similar mechanism of excitation/emission. The larger value observed for the RWLC-1 is due to a larger mixing ratio between the linear $^1A_1 \rightarrow {}^1A_2$ and plane polarized $^1A_1 \rightarrow {}^1E$ excitations. The limiting polarization case is that in which a linear excitation is followed by a linear emission oscillator giving rise to a polarization value of 0.5, similar to that observed for the RWLC-2 material. This would occur for a pure $^1A_1 \rightarrow {}^1A_2$ excitation with the linear component of the $^3E \rightarrow {}^1A_1$ emission.

Emission lifetimes

RuBpy encapsulated in RWLC-3 exhibits emission decays (Fig. 5, top panel) that best fit to a biexponential function (based upon χ^2 values and autocorrelation), with a fast phase τ-fast of 120 ns (58% of the total amplitude) and a slower phase τ-slow of 453 ns (42% of the total amplitude) at 25 °C (see Table 2 for a summary of the lifetime data). Attempts to fit

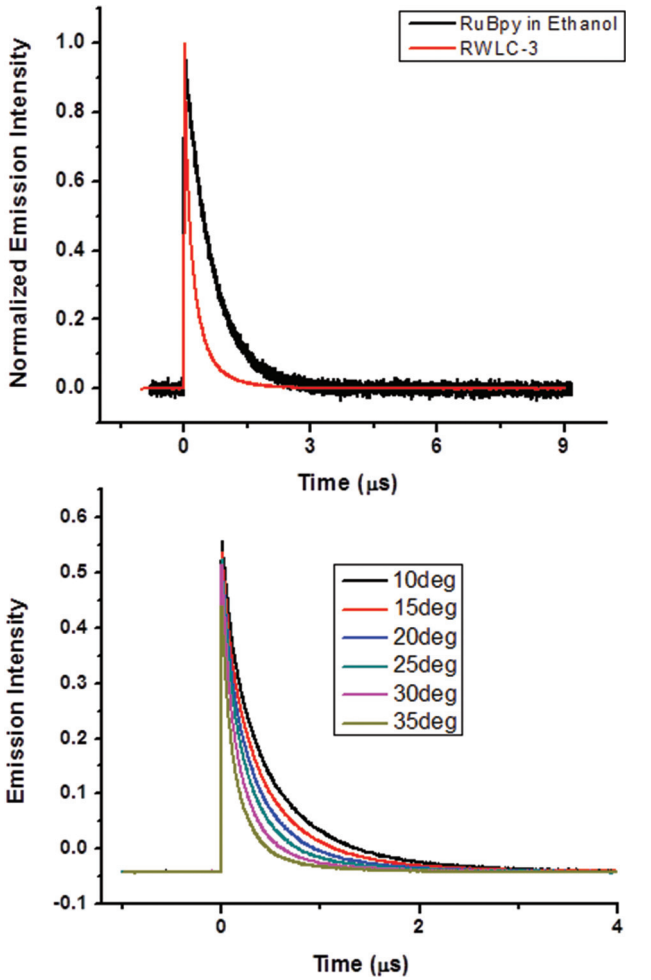

Fig. 5 Normalized time resolved emission decays of RWLC-3. Top panel: decay at 25 °C compared to RuBpy in solution. Bottom panel: overlay depicting temperature dependence. The emission decays of RWLC-3 fit to biexponential functions.

the emission decays to either a single exponential or stretched exponential function (probability distribution function) yielded poorer fits based upon χ^2 values. The lifetimes associated with each phase differs considerably from what is observed in solution or encapsulated in other MOF frameworks examined in our laboratory as well as RuBpy@zeoliteY.[18–21]

The general scheme for the excited state decay processes associated with RuBpy is summarized in Fig. 6.[8] The diagram illustrates both radiative and non-radiative pathways from a manifold of four closely spaced ^{3}MLCT states to the ground state as well as a non-radiative ligand field decay channel (^{3}LF). Three of the ^{3}MLCT states are separated by ~200 cm^{-1} and behave as a single state at room temperature while the fourth state lies ~400–1000 cm^{-1} above the three state manifold.[8] The observed emission decay rate constant can then be expressed as:

$$k_{obs} = k_0 + k_1 \exp(-\Delta E/RT) \quad (4)$$

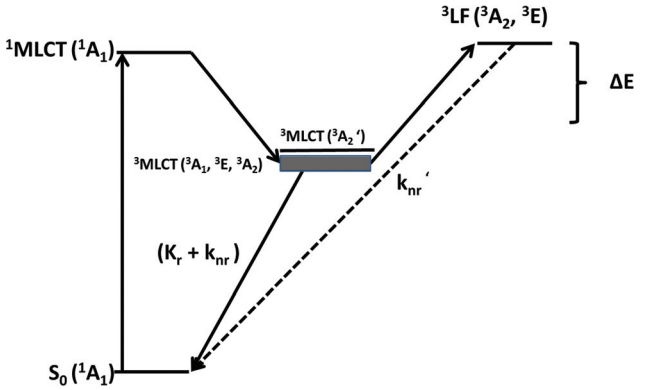

Fig. 6 Energy level diagram for RuBpy. The symmetry labels are for the D_3 symmetry complex.

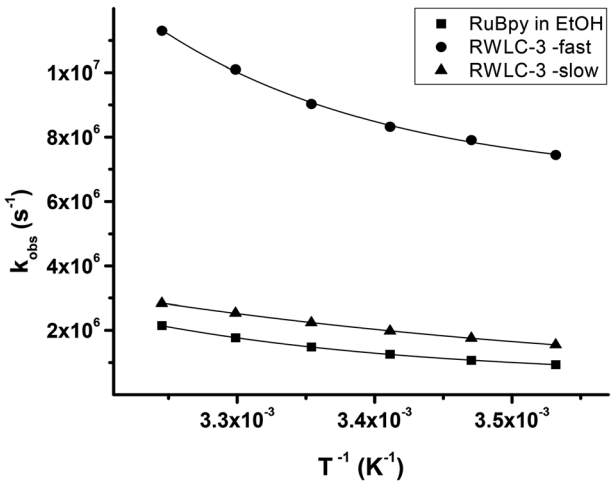

Fig. 7 Fits of the observed rate constants *versus* 1/*T* for RuBpy decay in solution and both phases of RWLC-3.

where k_{obs} is $1/\tau_{obs}$, $k_0 = k_r + k_{nr}$, k_r and k_{nr} are the radiative and non-radiative ^{3}MLCT decay rate constants, respectively, k_1 is the non-radiative decay rate constant from the ^{3}LF state and ΔE is the energy barrier between the ^{3}MLCT state and the ^{3}LF state. Fitting the emission decay lifetimes as a function of temperature (Fig. 7) to eqn (4) allows for the extraction of k_0, k_1 and ΔE for the RWLC-3 complex. The results are summarized in Table 3.

The results indicate two populations of RuBpy encapsulated within the RWLC-3 structure with photophysical parameters that are distinct from those observed for either the RWLC-1 or RWLC-2 structures, which also contain Zn MBBs and crystallographically resolvable RuBpy clusters.[5] The fast phase decay arises from an increase in both the k_0 and k_1 values by an order of magnitude over what is observed in RuBpy in solution. In addition, the k_1 value is also larger than those observed for the fast phases of RWLC-1 and RWLC-2 materials by roughly an order of magnitude while ΔE is similar to the RWLC-1, RWLC-2 and RuBpy (solution) values. These data suggest that the population of RuBpy giving rise to the fast

Table 3 Photophysical parameters from time resolved emission measurements obtained at 25 °C

Compound	k_0 ($s^{-1} \times 10^5$)	k_1 ($s^{-1} \times 10^{11}$)	ΔE (cm^{-1})	τ (ns)
RuBpy in EtOH	5.6	191	3491	676
RWLC-3-fast	53.9	1180	3624	120
RWLC-3-slow	2.9	0.1	1779	453
RWLC-2-fast[a]	39.8	125	3256	171
RWLC-2-slow[a]	7.6	0.2	2198	797
RWLC-1-fast[a]	38.3	267	3753	237
RWLC-1-slow[a]	5.3	0.2	2566	1600
RuBpy@USF2[b]	5.64	514	4593	1200
RuBpy@zeoliteY[c]	3.8	0.0011	890	530

[a] Data from ref. 4. [b] Data from ref. 3. [c] Data from ref. 16.

phase decay exhibits enhanced non-radiative decay pathways from both the ^{3}MLCT states and the ^{3}LF state without affecting the spacing between the two states. The most probable reason for the fast phase decay is the quenching of the ^{3}MLCT by co-encapsulated DEA molecules. Analysis of the X-ray structure reveals DMF and/or DEA molecules occupying the free space surrounding the RuBpy clusters within the framework cavities although the exact identity of the molecules could not be determined due to disorder. The presence of both fast and slow decay lifetimes is entirely consistent with a distribution of DMF/DEA molecules occupying space throughout the framework cavities with the fraction of DEA molecules being responsible for the fast phase quenching (DMF does not quench the RuBpy ^{3}MLCT). The population of RuBpy with nearby DMF molecules would then exhibit the longer phase decay.

The slow phase decay parameters for RWLC-3 are in between those observed for the RWLC-1 and RWLC-2 materials and RuBpy-encapsulated zeoliteY while being distinct from those of RuBpy@USF2 or RuBpy in solution.[4,5,18] For the RuBpy complex in solution thermal population of the ^{3}LF state results in an expansion of the RuBpy complex and rapid non-radiative relaxation.[22,23] Confinement within environments that restrict expansion, such as the USF2 MOF, results in an increase in ΔE and an increase in the observed emission lifetime (*i.e.*, deactivation of the non-radiate decay channel associated with the ^{3}LF state). In more extreme cases of confinement, such as the cavities associated with zeolite Y, the ΔE value for the ^{3}LF state increases well above the solution value such that the non-radiative deactivation through the ^{3}LF channel is no longer accessible.[18] In this case, the ΔE and k_1 values have been assigned to a fourth ^{3}MLCT state which lies ~900 cm^{-1} above the ^{3}MLCT manifold. The rate constant for the decay of the fourth ^{3}MLCT is on the order of 10^8, which restricts the observed decay lifetime to approximately 530 ns.

In the case of RWLC-1 and RWLC-2, the ΔE and k_1 values are distinct from RuBpy in solution and either of the RuBpy@USF2 or RuBpy@zeoliteY materials.[5,18] Specifically, lower values of ΔE would favour shorter radiative lifetimes due to increased population of the ^{3}LF state and enhanced non-radiative decay, which is not observed. Alternatively, the ΔE values

are much higher than would be expected for the energy barrier between the three state ^{3}MLCT manifold and the fourth ^{3}MLCT state (890 cm^{-1}). It has been suggested that RuBpy encapsulated within the RWLC-1 and RWLC-2 materials accesses MLCT states higher in energy than the fourth ^{3}MLCT state.[5] Computational studies have identified two singlet-in-character MLCT states that lie higher in energy than the fourth ^{3}MLCT state by 2450 cm^{-1} and 3100 cm^{-1}.[22] These states have also been observed experimentally at 2442 cm^{-1} and 3096 cm^{-1} above the fourth ^{3}MLCT state in single crystals of RuBpy(ClO$_4$)$_2$ [24] and are similar to the ΔE values determined for RWLC-1 and RWLC-2.[5] Although the decay rates for these states have not been previously reported, the k_1 values observed (2×10^{10} s^{-1}) are consistent with non-radiative decay.

The ΔE value for the slow phase decay of RWLC-3 is significantly lower than the solution value, only slightly lower than those observed for RWLC-1 and RWLC-2 and higher than that observed for the RuBpy@zeoliteY material.[5,18] In addition, the corresponding k_1 value is three orders of magnitude smaller than that observed for RuBpy in EtOH but near that of the RWLC-1 and RWLC-2 materials, which are both two orders of magnitude larger than the RuBpy@zeoliteY value. This would suggest one of two possibilities for the slow phase photophysics of RWLC-3. First, the ^{3}LF state is raised in energy due to confinement well above the ^{3}MLCT manifold and the ΔE value reflects the barrier of one of the two ^{1}MLCT states that has been lowered in energy due to the environment of the MOF cavities. If this is the case then the cavity environment also lowers the value of k_0 (presumably the k_{nr} component) as well as k_1, resulting in a τ value significantly smaller than that observed for either RWLC-1 or RWLC-2. An alternative possibility is that the ^{3}LF state increases in energy prohibiting significant population (as above), allowing instead for the population of the fourth ^{3}MLCT state, as observed in the RuBpy@zeoliteY material.[18] However, the fourth ^{3}MLCT is increased in energy by ~900 cm^{-1} relative to RuBpy@zeoliteY and with enhanced non-radiative decay channels that are likely due to interactions with the framework atoms. Computational efforts are underway in order to determine which of the two possibilities reflects the disposition of the RuBpy slow phase in the RWLC-3 material.

Conclusion

The data presented here demonstrate the ability to template a new metal organic framework material with unique photophysical properties. Specifically, the reaction of Zn(II) with 1,4-BDC in the presence of RuBpy produces an interpenetrated MOF containing crystallographically resolvable RuBpy clusters encapsulated within the MOF cavities. The photophysical properties of the encapsulated RuBpy are unique relative to other RuBpy-containing MOFs. The RuBpy clusters appear to be distributed within two environments, one in which the ^{3}MLCT is quenched by an exogenous donor and the second that modulates the ^{3}LF state (due to the restricted cavity size) resulting in the population of either a ^{1}MLCT or a fourth ^{3}MLCT both of which have distinct properties relative to other RuBpy systems. Overall, the results presented here illustrate the ability of the MOF frameworks to modulate the excited states of guest molecules which are of key importance in the design of MOFs with enhanced photocatalytic properties.

Acknowledgements

The authors would like to acknowledge the University of South Florida Office of Research and Innovation for support of this work. Crystal diffraction studies of RWLC-3 MOF were carried out at the Advanced Photon Source on beam line 15ID-C of ChemMatCARS Sector 15, which is principally supported by the National Science Foundation/Department of Energy under grant number NSF/CHE-0822838. Use of the Advanced Photon Source was supported by the U. S. Department of Energy, Office of Science, Office of Basic Energy Sciences, under contract no. DE-AC02-06CH11357.

Notes and references

1 H.-C. Zhou, J. R. Long and O. M. Yaghi, *Chem. Rev.*, 2012, **112**, 673–674; B. Moulton and M. J. Zaworotko, *Chem. Rev.*, 2001, **101**, 1629–1658; M. Eddaoudi, D. B. Moler, H. Li, B. Chen, T. M. Reinke, M. O'Keeffe and O. M. Yaghi, *Acc. Chem. Res.*, 2001, **34**, 319–330; J.-R. Li, J. Sculley and H.-C. Zhou, *Chem. Rev.*, 2012, **112**, 869–932; P. Horcajada, R. Gref, T. Baati, P. K. Allen, G. Maurin, P. Couvreur, G. Férey, R. E. Morris and C. Serre, *Chem. Rev.*, 2012, **112**, 1232–1268.

2 T. Zhang and W. Lin, *Chem. Soc. Rev.*, 2014, **43**, 5982–5993; J.-L. Wang, C. Wang and W. Lin, *ACS Catal.*, 2012, **2**, 2630–2640; M. A. Nasalevich, M. van der Veen, F. Kapteijn and J. Dascon, *CrystEngComm*, 2014, **16**, 4919–4926; F. L. Xamena and G. Gascon, *Metal Organic Frameworks as Heterogeneous Catalysts*, RSC Catalysis Series, RSC Publishing, 2013; S. Saha, G. Das, J. Thote and R. Banerjee, *J. Am. Chem. Soc.*, 2014, **136**, 14845–14851; J. R. Choi, T. Tachikawa, M. Fujitsuka and T. Majima, *Langmuir*, 2010, **26**, 10437–10443.

3 M. H. Alkordi, Y. Liu, R. W. Larsen, J. F. Eubank and M. Eddaoudi, *J. Am. Chem. Soc.*, 2008, **130**, 12639–12641; R. W. Larsen, L. Wojtas, J. Perman, R. L. Musselman, M. J. Zaworotko and C. M. Vetromile, *J. Am. Chem. Soc.*, 2011, **133**, 10356–10359; R. W. Larsen, J. Miksovska, R. L. Musselman and L. Wojtas, *J. Phys. Chem. A*, 2011, **115**, 11519–11524; Z. Zhang, L. Zhang, L. Wojtas, P. Nugent, M. Eddaoudi and M. J. Zaworotko, *J. Am. Chem. Soc.*, 2012, **134**, 924–927; Z. Zhang, L. Wojtas and M. J. Zaworotko, *Cryst. Growth Des.*, 2014, **14**, 1526–1530.

4 R. W. Larsen and L. Wojtas, *J. Phys. Chem. A*, 2012, **116**, 7830–7835.

5 C. L. Whittington, L. Wojtas and R. W. Larsen, *Inorg. Chem.*, 2014, **53**, 160–166.
6 Y. Komada, S. Yamauchi and N. Hirota, *J. Phys. Chem.*, 1988, **92**, 6511–6518; W. A. Maza and A. J. Morris, *J. Phys. Chem. C*, 2014, **118**, 8803–8817.
7 M. D. Allendorf, C. A. Bauer, R. K. Bhakta and R. J. T. Houk, *Chem. Soc. Rev.*, 2009, **38**, 1330–1352; Y. Cui, Y. Yue, G. Qian and B. Chen, *Chem. Rev.*, 2012, **112**, 1126–1162; Y. Cui, B. Chen and G. Qian, *Coord. Chem. Rev.*, 2014, **273–274**, 76–86; Y. Cui, Y. Yue, G. Qian and B. Chen, *Chem. Rev.*, 2012, **112**, 1126–1162; Y. Chen and S. Ma, *Coord. Chem. Rev.*, 2012, **32**, 81–100; D. Yan, Y. Tang, H. Lin and D. Wang, *Nature*, 2013, **4**, 4437.
8 N. Sutin and C. Creutz, *Pure Appl. Chem.*, 1980, **52**, 2717–2738; T. J. Meyer, *Pure Appl. Chem.*, 1986, **58**, 1193–1206; D. W. Thompson, A. Ito and T. J. Meyer, *Pure Appl. Chem.*, 2013, **85**, 1257–1305; S. R. Allsop, A. Cox, S. H. Jenkins, T. J. Kemp and S. M. Tunstal, *Chem. Phys. Lett.*, 1976, **43**, 135; H. Yersin and E. Gallhuber, *J. Am. Chem. Soc.*, 1984, **106**, 8117.
9 L.-G. Qiu, T. Xu, Z.-Q. Li, W. Wang, Y. Wu, X. Jiang, X.-Y. Tian and L.-D. Zhang, *Angew. Chem., Int. Ed.*, 2008, **47**, 9487–9491.
10 Z. Xin, J. Bai, Y. Pan and M. J. Zaworotko, *Chem. – Eur. J.*, 2010, **16**, 13049–13052.
11 *APEX2*, Bruker-AXS Inc., Madison, WI, USA, 2010.
12 G. M. Sheldrick, *Acta Crystallogr., Sect. A: Found. Crystallogr.*, 2008, **64**, 112–122.
13 J. V. Casper and T. J. Meyer, *J. Am. Chem. Soc.*, 1983, **105**, 5583–5590.
14 D. M. Jameson, in *Introduction to Fluorescence*, CRC Press, Boca Raton, FL, USA, 1st edn, 2014.
15 I. Fujita and H. Kobayashi, *Inorg. Chem.*, 1973, **12**, 2758–2762.
16 F. Felix, J. Ferguson, H. U. Guedel and A. Ludi, *J. Am. Chem. Soc.*, 1980, **102**, 4096–4102.
17 J. van Houten and R. J. Watts, *J. Am. Chem. Soc.*, 1976, **98**, 4853–4858.
18 K. Maruszewski, D. P. Strommen and J. R. Kincaid, *J. Am. Chem. Soc.*, 1993, **115**, 8345–8350.
19 J. A. Incavo and P. K. Dutta, *J. Phys. Chem.*, 1990, **94**, 3075–3081.
20 P. Lainé, M. Lanz and G. Calzaferri, *Inorg. Chem.*, 1996, **35**, 3514–3518.
21 J. V. Caspar and T. J. Meyer, *J. Am. Chem. Soc.*, 1983, **105**, 5583–5590.
22 K. R. Bargawi, A. Llobet and T. J. Meyer, *J. Am. Chem. Soc.*, 1988, **110**, 7751–7759.
23 J.-L. Heully, F. Alary and M. Boggio-Pasqua, *J. Chem. Phys.*, 2009, **131**, 184308.
24 Y. Komada, S. Yamauchi and N. Hirota, *J. Phys. Chem.*, 1988, **92**, 6511–6518.